Research articles

Novel Fe-based nanocrystalline powder cores with excellent magnetic properties produced using gas-atomized powder

Liang Chang [a,c], Lei Xie [a,c], Min Liu [c], Qiang Li [a,*], Yaqiang Dong [c,*], Chuntao Chang [b,c,*], Xin-Min Wang [c], Akihisa Inoue [c]

[a] School of Physics Science and Technology, Xinjiang University, Urumqi, Xinjiang 830046, China
[b] School of Mechanical Engineering, Dongguan University of Technology, Dongguan 523808, China
[c] Zhejiang Province Key Laboratory of Magnetic Materials and Application Technology, Key Laboratory of Magnetic Materials and Devices, Ningbo Institute of Materials Technology & Engineering, Chinese Academy of Sciences, Ningbo, Zhejiang 315201, China

ARTICLE INFO

ABSTRACT

FeSiBPNbCu nanocrystalline powder cores (NPCs) with excellent magnetic properties were fabricated by cold-compaction of the gas-atomized amorphous powder. Upon annealing at the optimum temperature, the NPCs showed excellent magnetic properties, including high initial permeability of 88, high frequency stability up to 1 MHz with a constant value of 85, low core loss of 265 mW/cm^3 at 100 kHz for B_m = 0.05 T, and superior DC-bias permeability of 60% at a bias field of 100 Oe. The excellent magnetic properties of the present NPCs could be attributed to the ultrafine α-Fe(Si) phase precipitated in the amorphous matrix and the use of gas-atomized powder coated with a uniform insulation layer.

© 2017 Elsevier B.V. All rights reserved.

1. Introduction

As magnetic components, magnetic powder cores (MPCs) have been widely used in noise suppressors, inductor and other reactors in electromagnetic devices, etc. [1–4]. MPCs are produced by the compaction of ferromagnetic powder particles that are insulated electrically with one another by an organic and/or inorganic insulation layer on the powder surface before powder compaction process. Further developments to electromagnetic devices are aimed at achieving high frequency, miniaturization, and noise reduction. Since conventional MPCs cannot meet the above requirements [5,6], development of novel MPCs with excellent soft magnetic properties is an urgent issue.

Fe-based amorphous alloys have been reported to exhibit excellent soft magnetic properties [7,8], which are suitable for the production of MPCs with high performance [9]. However, the audible load/no-load noise caused by large magnetostriction (λ_s) restricts the application of the powder cores fabricated using Fe-based amorphous alloys [10,11]. In contrast, Fe-based nanocrystalline alloys consisting of ultrafine α-Fe(Si) grains embedded in the residual amorphous matrix show nearly zero λ_s and exhibit excellent soft magnetic properties over a range of high frequency, including high saturation magnetization (M_s) and low coercivity (H_c) [12–14], which can be used to prepare high-performance nanocrystalline powder cores (NPCs) without load/no-load noise.

NPCs are generally fabricated using the flake powder produced by ribbon pulverization, due to the glass forming ability (GFA) of conventional nanocrystalline alloys [15–17]. However, undesirable breakdown of the insulation layer at the irregular corners and sharp edges of the flake powder may result from the high pressure during the cold compaction process, which leads to an increase in core loss and unstable soft magnetic performance [18]. Meanwhile, the ferromagnetic resonance Kittel formula indicates that the resonance frequency decreases as the demagnetization coefficients decrease. Thus, the resonance frequency decreases as the particle shape becomes flat, which also restricts the application of NPCs at high frequencies [19]. The issue caused by flake powder can be effectively resolved if the NPCs can be fabricated using spherical amorphous alloy powder, which in turn is obtained by the gas atomization method. However, in order to prepare amorphous alloy powder by gas atomization, the alloy must show sufficiently high GFA.

In our previous work, we have successfully developed a new Fe-based nanocrystalline alloy with the composition $(Fe_{0.76}Si_{0.09}B_{0.1}P_{0.05})_{98.5}Nb_1Cu_{0.5}$ [20], which exhibits high GFA (d_{max} = 2.5 mm), high B_s (1.46 T), and low H_c (2.8 A·m^{-1}). In the present study, $(Fe_{0.76}Si_{0.09}B_{0.1}P_{0.05})_{98.5}Nb_1Cu_{0.5}$ spherical powder with a fully

* Corresponding authors at: School of Mechanical Engineering, Dongguan University of Technology, Dongguan 523808, China (C. Chang).

E-mail addresses: qli@xju.edu.cn (Q. Li), dongyq@nimte.ac.cn (Y. Dong), ctchang@nimte.ac.cn (C. Chang).
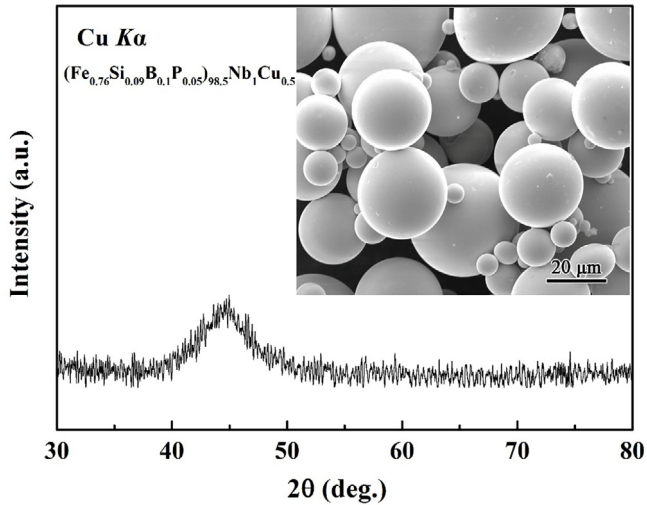
Fig. 1. XRD patterns of the as-quenched FeSiBPNbCu gas-atomized powder; the inset shows the morphology of the as-quenched FeSiBPNbCu powder.

Fig. 2. DSC curves of the as-quenched powder and melt-spun ribbon.

amorphous phase was prepared by gas atomization. The corresponding FeSiBPNbCu MPCs were fabricated by cold compaction of the gas atomization amorphous powder, and the NPCs were obtained by annealing the MPCs at the appropriate condition. The magnetic properties of the resulting FeSiBPNbCu powder cores were investigated systematically.

2. Experiment

A multicomponent alloy ingot with the nominal composition $(Fe_{0.76}Si_{0.09}B_{0.1}P_{0.05})_{98.5}Nb_1Cu_{0.5}$ was prepared by induction melting of a mixture of high-purity metals including Fe, Nb, and Cu; crystalline B and Si metalloids; and Fe_3P pre-alloy in a high-purity argon atmosphere. Metallic powder with a fully amorphous phase and particle size ranging up to 75 μm was prepared by gas atomization. The powder was uniformly mixed with 2 wt% epoxy resin as an organic binder. Toroidal powder cores had dimensions of $\Phi 20.3 \times \Phi 12.7 \times t5.4$ mm were prepared by compaction of the powder mixture via cold pressing under 1.8 GPa pressure. Finally, the powder cores were annealed at 400, 480, 490, and 500 °C for 0.5 h in vacuum. The characteristics of the FeSiBPNbCu gas-atomized powder were analyzed by differential scanning calorimetry (DSC) and scanning election microscopy (SEM). The microstructures of the gas-atomized powder and as-annealed powder cores were examined by X-ray diffraction (XRD) with Cu $K\alpha$ radiation. It is very difficult to prepare transition electron microscopy (TEM) specimens using powders with such a small particle size. Hence, melt-spun ribbons with the same composition as that of the present gas-atomized powder, annealed under the same conditions as those for the present NPCs were employed for TEM observations. The M-H loops of the as-annealed powder cores were measured using a vibrating sample magnetometer (VSM). The real part of complex permeability of the as-annealed powder cores was calculated from the core inductance, which is measured by an Agilent 4294A impedance analyzer from 1 kHz to 110 MHz. The DC-bias field performance was measured by an Agilent 4284A LCR meter; the total core loss was measured by an alternating current (AC) B-H loop analyzer; and the hysteresis loss was measured by a direct current (DC) B-H loop analyzer. Additionally, the density of the samples was determined by the Archimedes immersion method using the distilled water as working liquid.
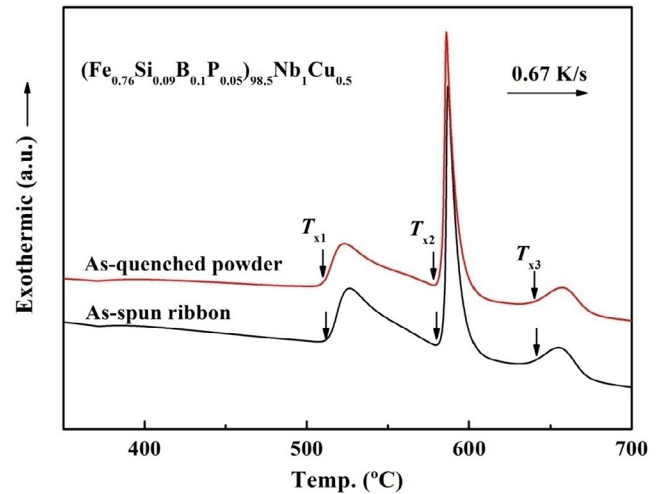
3. Results and discussion

Fig. 1 shows the XRD pattern of the as-quenched FeSiBPNbCu gas-atomized powder. The XRD pattern of the powder exhibits only a broad diffuse peak, indicating a fully amorphous structure within the sensitivity of XRD measurement. The inset of Fig. 1 shows the morphology of the as-quenched FeSiBPNbCu gas-atomized powder with the particle size ranging up to 75 μm. No appreciable contrast, that would indicate the formation of a crystalline phase, is seen on the outer surface of any particle. The powders are spherical in shape, which is more favorable for the uniform insulation coating, thereby reducing the eddy current loss between the powders.

Fig. 2 shows the DSC curve of the as-quenched FeSiBPNbCu gas-atomized powder, together with the data for the melt-spun glassy alloy ribbon for comparison. The DSC curve of the gas-atomized powder exhibits three exothermic peaks. The onset temperatures of the first, second, and third exothermic peaks are 516, 583, and 641 °C, marked as T_{x1}, T_{x2}, and T_{x3}, respectively. No appreciable difference in the crystallization process is observed between the powder and the melt-spun ribbon. Additionally, the total crystallization enthalpy ($\Sigma\Delta H_x$) of the samples is determined from the DSC curve. The value of $\Sigma\Delta H_x$ for the gas-atomized powder is 5.8 kJ/mol and is close to that (6.2 kJ/mol) of the melt-spun ribbon, which further confirms the amorphous nature of the gas-atomized powder.

The annealing temperatures for the powder cores fabricated by cold compaction of the gas-atomized amorphous powder are determined based on the DSC thermal scans. The XRD patterns of the as-prepared FeSiBPNbCu powder core and the corresponding powder cores annealed at different temperatures are shown in Fig. 3. The as-prepared and annealed (at 400 °C) powder cores exhibit a fully amorphous phase and are denoted as amorphous powder cores (APCs) in the following discussion. Three diffraction peaks attributed to the (1 1 0), (2 0 0), and (2 1 1) lattice planes of the α-Fe(Si) phase, respectively, appear in the XRD patterns of the powder cores annealed at 480 and 490 °C, which are denoted as nanocrystalline powder cores (NPCs). The grain size of the α-Fe(Si) phase in the NPCs obtained by annealing at 480 and 490 °C is estimated to be about 22 and 24 nm, respectively, according to the Scherer formula. The XRD pattern of the powder core annealed at 500 °C (Fig. 3) shows diffraction peaks corresponding to the α-Fe(Si), $Fe_3(B,P)$, and Fe_2B phases, indicating that these phases precipitate simultaneously, thus deteriorating the soft magnetic properties of the powder cores [21].
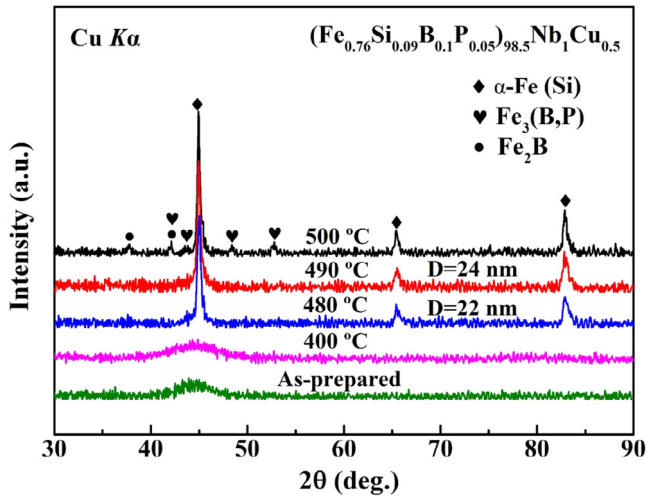
Fig. 3. XRD patterns of the as-prepared FeSiBPNbCu powder core and corresponding powder cores annealed at different temperatures.

Fig. 5. Frequency dependence of permeability for FeSiBPNbCu powder cores annealed at different temperatures.

The nanocrystalline structure of the annealed samples is further confirmed by TEM observations. Fig. 4 presents the TEM image of the melt-spun ribbon after annealing at 480 °C for 0.5 h, wherein the α-Fe(Si) grains are identified from the selected-area electron diffraction (SAED) patterns, as shown in the inset of Fig. 4. These grains have an average size of approximately 22 nm and are randomly dispersed in the residual amorphous matrix. Because the local anisotropies are randomly averaged out by the grains within the ferromagnetic exchange length, small nanocrystals homogeneously embedded in the amorphous matrix are favorable for achieving good soft magnetic properties in the case of nanocrystalline soft magnetic materials [22]. Compared to their amorphous counterparts, the corresponding nanocrystallized alloys exhibit lower λ_s, higher effective permeability (μ_e), and higher B_s [23,24]. The low λ_s can effectively reduce the audible noise of MPCs that is generated during the application.
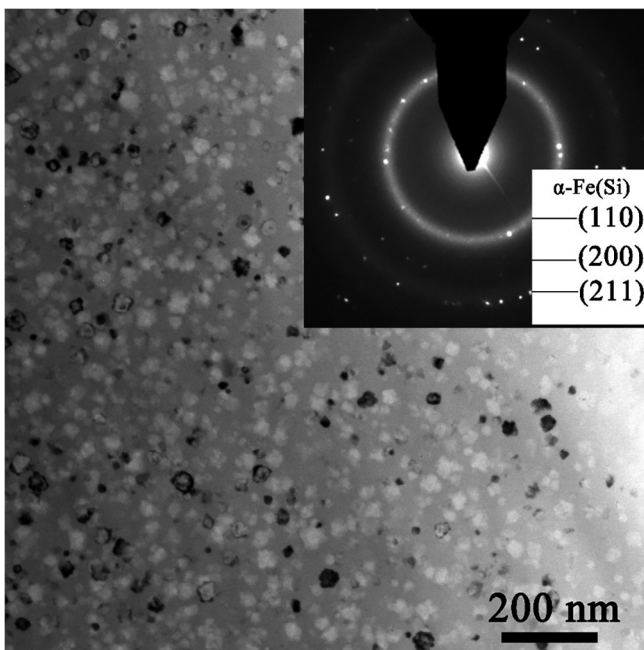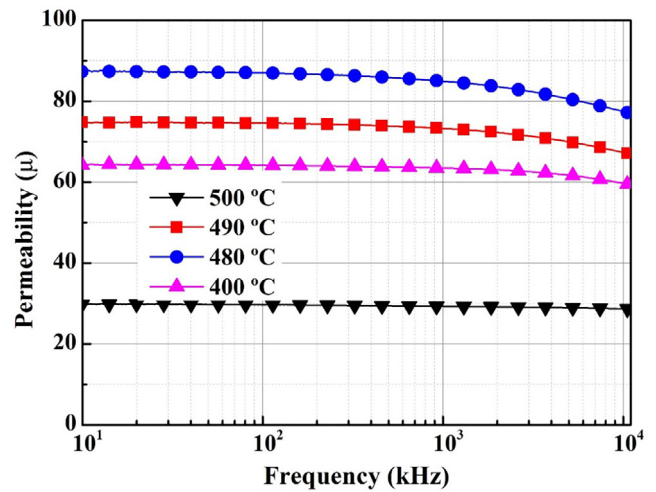
Fig. 5 shows the frequency dependence of permeability for the FeSiBPNbCu powder cores annealed at different temperatures. The APCs exhibit a good high-frequency characteristic of permeability, which keeps at a value of 65 up to 1 MHz. The permeability, however, is obviously improved for the NPCs obtained by annealing at 480 and 490 °C. In particular, the NPCs annealed at 480 °C exhibit the highest initial permeability of 88 and retain a stable permeability of 85 up to 1 MHz frequency. Moreover, all specimens exhibit excellent high-frequency stability up to about 1 MHz, mainly because the non-magnetic inorganic insulating layer decreases the volume fraction of the ferromagnetic particles in the MPCs, providing the equivalent of a distributed air gap, which leads to an increase in the relaxation frequency. The permeability (μ) can generally be calculated according to the Ollendorf's formula as Eq. (1) [25]:

$$\mu = \frac{\eta\mu_0(\mu_t - \mu_0)}{[N(1 - \eta)(\mu_t - \mu_0) + \mu_0]} + \mu_0 \tag{1}$$

where η is the packing density, N is the demagnetizing coefficient, μ_t is intrinsic permeability of material, and μ_0 is the vacuum permeability. The μ_t of FeSiBPNbCu amorphous alloy and nanocrytalline alloy should be much larger than μ_0, thus the permeability of the powder core is determined only by the η and N according to Eq. (1). Here the N can be considered same for all the present powder cores. The η of the powder core can be calculated as the ratio of the density of the powder core to the density of the FeSiBPNbCu master ingot. The density of the master ingot and the powder cores obtained by annealing at 400, 480, 490 and 500 °C is measured to be 7.35, 5.38, 5.58, 5.52 and 5.51 g/cm³, respectively. So the η of the powder cores annealed at 400, 480, 490 and 500 °C is determined to be 73.2%, 75.9%, 75.1% and 74.9%, respectively. It can see that the packing density of the powder cores improves as the increase of the annealing temperature, which leads to the increase of the permeability of the powder cores. Additionally, in fact the η in Eq. (1) should refer to the packing density of the soft magnetic phase. As mentioned previous, besides α-Fe(Si) phase, a certain amount of $Fe_3(B,P)$ and Fe_2B phases are precipitated in the NPC annealed at 500 °C and thus the effective packing density should be lower than the measure value of 74.9%. Therefore, the NPC annealed at 500 °C has a lower permeability compared with the NPCs annealed at 480 and 490 °C.

The M-H loops of the APCs and NPCs by VSM measurements are show in Fig. 6. It can see that the M_s of the APC is 148 emu/g, and the M_s of the NPCs annealed at 480 and 490 °C has an obvious

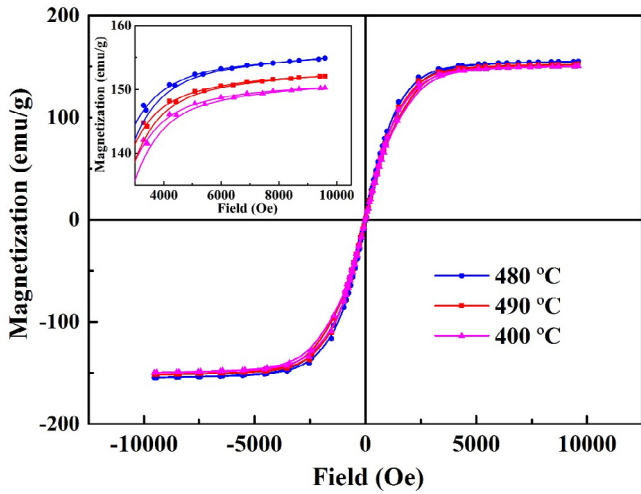**Fig. 4.** TEM image and SAED pattern of the melt-spun ribbon after annealing at 480 °C for 0.5 h.

Fig. 6. *M-H* loop of FeSiBPNbCu powder cores annealed at different temperatures.

increase and reaches 155 and 152 emu/g, respectively, which should be attributable to the ultrafine α-Fe(Si) phase precipitated after annealing [23,24].

Fig. 7 presents the frequency dependence of core loss for the FeSiBPNbCu powder cores annealed at different temperatures. The APCs show a low core loss of 475 mW/cm^3 at 100 kHz for $B_m = 50$ mT. As compared with the APCs, the core loss of the NPCs obviously decreases and the NPC annealed at 480 °C exhibits the lowest core loss of 265 mW/cm^3. When the annealing temperature is increased to 500 °C, the core loss of the specimens shows a substantial increase. Generally, the core loss includes hysteresis loss (P_h), eddy current loss (P_e), and residual loss (P_r). The residual loss is a combination of relaxation and resonant losses of the system, which is important only at very low induction levels and very high frequencies and can be ignored in power applications. Then, the core loss of MPCs is expressed as the sum of the P_h and P_e, provided changes in the magnetic field inside the material are not accompanied by relaxation phenomena (magnetic resonance, etc.) in the studies range [2]. Hence, both the APCs and NPCs exhibit low core loss due to the uniform insulation layers coated on the powder surface, which provide a relatively high resistivity to the MPCs and can effectively reduce the P_e. Compared with the APCs, the NPCs exhibit lower core loss because of the decrease in P_h, which is
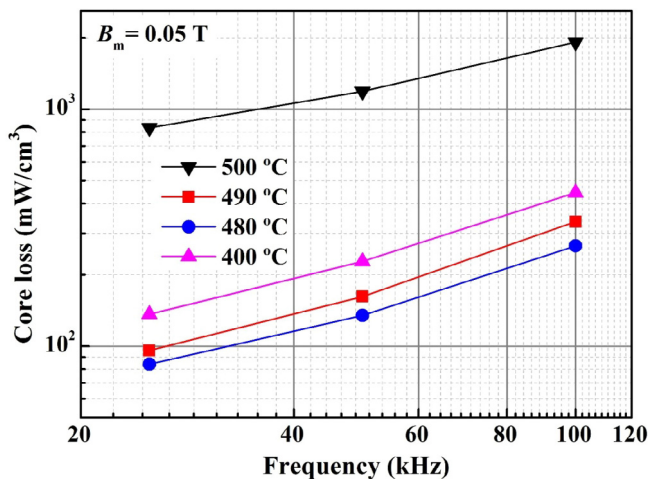
affected by the H_c value of the material. That is, the lower H_c, the lower will P_h be [26,27].

P_h is defined as the energy absorbed by the material as the AC magnetic field sweeps around the hysteresis curve and can be described as the energy required to sweep the domain walls. In addition, P_h can be obtained by extrapolating the corresponding conversion loss (loop area) in a static magnetic field. Thus, the hysteresis loop area of the specimens swept out in a DC magnetic field, which is based on the AC hysteresis curve ($B_m = 50$ mT, $f = 50$ kHz), is shown in Fig. 8(a). The H_c value is much lower for the NPCs than for the APCs and the specimens annealed at 500 °C. The DC hysteresis loop area has the same representation as H_c. Furthermore, the contribution of P_h and P_e (50 mT, 50 kHz) has been investigated, as shown in Fig. 8(b). P_e decreases slightly when the annealing temperature is increased from 400 °C to 480 and 490 °C, and increases substantially as the temperature is further increased to 500 °C. P_h, however, decreases significantly from 67 mW/cm^3 to 6 and 8 mW/cm^3 when the annealing temperature is increased from 400 °C to 480 and 490 °C, respectively. With a further increase in the annealing temperature to 500 °C, P_h experiences a substantial increase to 302 mW/cm^3. Thus, the decrease in P_h caused by the lower H_c is the principal reason for the decrease in total core loss of the NPCs as compared with the case of the APCs, which is consistent with the discussion above. However, P_e plays a dominant role in core loss at high frequencies [28], and thus the decrease in P_e is a reasonable explanation for the increased permeability.
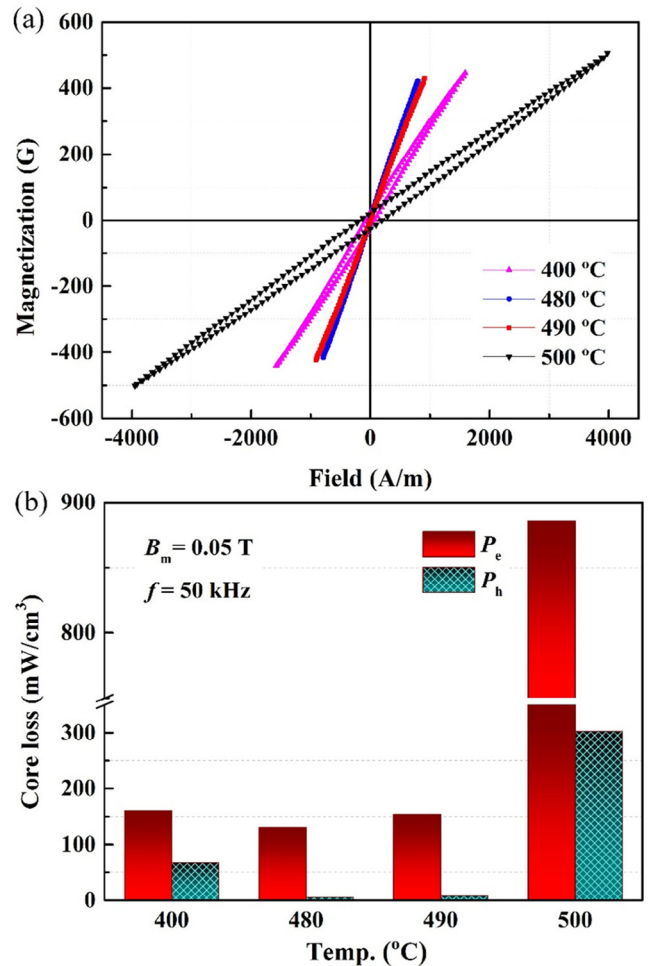

Fig. 8. (a) DC hysteresis loop of FeSiBPNbCu powder cores annealed at different temperatures, (b) Separation of total loss into P_e and P_h for samples prepared at different annealing temperatures.

Fig. 7. Frequency dependence of core loss for FeSiBPNbCu powder cores annealed at different temperatures.
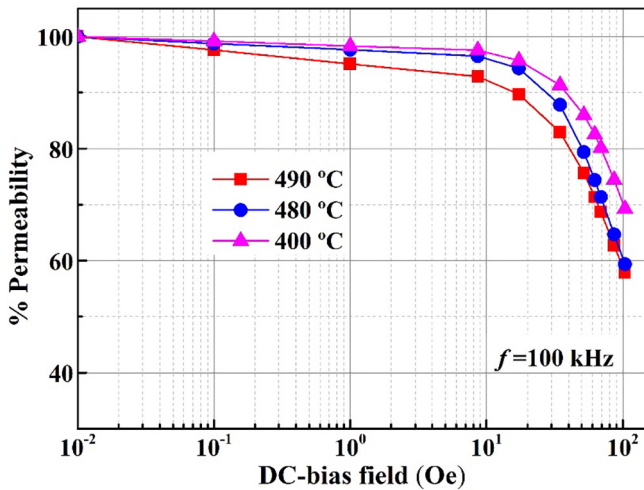
Fig. 9. Percentage of permeability with DC-bias field at 100 kHz for FeSiBPNbCu powder cores annealed at different temperatures.

The DC level must be tolerated for MPCs in many applications; hence, the core material must exhibit a high incremental permeability (μ_Δ) (also known as reversible permeability μ_{rev} when the AC magnetic field is very small) at a higher DC bias magnetic field H_{DC} (the so-called DC bias property) [29,30]. The permeability measured with a superimposed DC tends to pre-magnetize the MPCs, so that the inductance is reduced. The inductance will progressively decrease as the DC-bias field is increased, and the MPCs approach saturation. The DC-bias field dependence of the percent permeability for the annealed FeSiBPNbCu powder cores at 100 kHz is shown in Fig. 9. The APCs exhibit a high μ_Δ of 70% at $H =$ 100 Oe. The μ_Δ value of the NPCs is slightly lower than that of the APCs but still remains at a high level. The NPCs annealed at 480 °C, in particular, exhibit high permeability and a superior μ_Δ of 60%, implying that the FeSiBPNbCu NPCs are not easily saturated under the applied magnetic field.

4. Conclusions

The magnetic properties of FeSiBPNbCu powder cores fabricated using gas-atomized powder with a fully amorphous phase have been investigated. The NPCs obtained through annealing at 480 °C for 0.5 h exhibit excellent magnetic properties, including a high initial permeability of 88, frequency stability up to 1 MHz with a constant value of 85, low core loss ($P_{cv\ (0.05/100)} = 265$ mW/cm^3), and superior DC-bias property of about 60% at $H = 100$ Oe. The excellent magnetic performance of the present NPCs is mainly due to the precipitation of an ultrafine α-Fe(Si) phase with a homogeneous grain size distribution in the residual amorphous matrix after appropriate annealing treatment, and the uniform insulation layer of the gas-atomized powder.

References

[1] K.K. Oh, H. Lee, W.S. Lee, M.J. Yoo, W.N. Kim, H.G. Yoon, Effect of viscosity on the magnetic permeability of Sendust-filled polymer composites, J. Magn. Magn. Mater. 321 (2009) 1295–1299.
[2] Y.P. Liu, Y.D. Yi, W. Shao, Y.F. Shao, Microstructure and magnetic properties of soft magnetic powder cores of amorphous and nanocrystalline alloys, J. Magn. Magn. Mater. 330 (2013) 119–133.
[3] X.A. Fan, Z.Y. Wu, G.Q. Li, J. Wang, Z.D. Xiang, Z.H. Gan, High resistivity and low core loss of intergranular insulated Fe-6.5wt.%Si/SiO$_2$ composite compacts, Mater. Des. 89 (2016) 1251–1258.
[4] Y.D. Peng, Y. Yi, L.Y. Li, J.H. Yi, J.W. Nie, C.X. Bao, Iron-based soft magnetic composites with Al$_2$O$_3$ insulation coating produced using sol-gel method, Mater. Des. 109 (2016) 390–395.
[5] D. Liu, C. Wu, M. Yan, Investigation on sol-gel Al$_2$O$_3$ and hybrid phosphate-alumina insulation coatings for FeSiAl soft magnetic composites, J. Mater. Sci. 50 (2015) 6559–6566.
[6] W. Ding, L.T. Jiang, Y.Q. Liao, J.B. Song, B.Q. Li, G.H. Wu, Effect of iron particle size and volume fraction on the magnetic properties of Fe/silicate glass soft magnetic composites, J. Magn. Magn. Mater. 378 (2015) 232–238.
[7] S. Yoshida, T. Mizushima, T. Hatanai, A. Inoue, Preparation of new amorphous powder cores using Fe-based glassy alloy, IEEE. Trans. Magn. 36 (2000) 3424–3429.
[8] R. Hasegawa, R.E. Hathaway, C.F. Chang, Magnetic-properties of consolidated glassy metal-powder cores, J. Appl. Phys. 57 (1985) 3566–3568.
[9] E.Y. Kang, Y.B. Kim, K.Y. Kim, Y.H. Chung, H.K. Baik, Preparation of Fe-Si-B-Nb amorphous powder cores with excellent high-frequency magnetic properties, J. Magn. Magn. Mater. 304 (2006) 182–185.
[10] D. Azuma, R. Hasegawa, Audible noise from amorphous metal and silicon steel-based transformer core, IEEE Trans. Magn. 47 (2011) 3460–3462.
[11] Y. Ogawa, M. Naoe, Y. Yoshizawa, R. Hasegawa, Magnetic properties of high B_s Fe-based amorphous material, J. Magn. Magn. Mater. 304 (2006) 675–677.
[12] Y. Yoshizawa, S. Oguma, K. Yamauchi, New Fe-based soft magnetic alloys composed of ultrafine grain structure, J. Appl. Phys. 64 (1988) 6044–6046.
[13] G. Herzer, Grain-structure and magnetism of nanocrystalline ferromagnets, IEEE Trans. Magn. 25 (1989) 3327–3329.
[14] M. Hasiak, W.H. Ciurzynska, Y. Yamashiro, Microstructure and some magnetic properties of amorphous and nanocrystalline Fe-Cu-Nb-Si-B alloys, Mater. Sci. Eng. A 293 (2000) 261–266.
[15] E.K. Cho, X.T. Kwon, E.M. Cho, Y.S. Song, K.Y. Sohn, W.W. Park, The control of nano-grain size and magnetic properties of Fe$_{73}$Si$_{16}$B$_7$Nb$_3$Cu$_1$ soft magnetic powder cores, Mater. Sci. Eng. A 449–451 (2007) 368–370.
[16] G.H. Kim, T.H. Noh, G.B. Choi, K.Y. Kim, Magnetic properties of FeCuNbSiB nanocrystalline alloy powder cores using ball-milled powder, J. Appl. Phys. 93 (2003) 7211–7213.
[17] T.H. Kim, K.K. Jee, Y.B. Kim, D.J. Byun, J.H. Han, High-frequency magnetic properties of soft magnetic cores based on nanocrystalline alloy powder prepared by thermal oxidation, J. Magn. Magn. Mater. 322 (2010) 2423–2427.
[18] H.Y. Choi, S.J. Ahn, T.H. Noh, Magnetic properties of nanocrystalline Fe$_{73.5}$Cu$_1$Nb$_3$Si$_{15.5}$B$_7$ alloy powder cores with different particle size prepared by rotor mill, Phys. Status Solidi A 201 (2004) 1879–1882.
[19] F. Alves, C. Ramiarinjaona, S. Berenguer, R. Lebourgeois, T. Waeckerle, High-frequency behavior of magnetic composites based on FeSiBCuNb particles for power electronics, IEEE Trans. Mag. 38 (2002) 3135–3137.
[20] Z.Z. Li, A.D. Wang, C.T. Chang, Y.G. Wang, B.S. Dong, S.X. Zhou, FeSiBPNbCu alloys with high glass-forming ability and good soft magnetic properties, Intermetallics 54 (2014) 225–231.
[21] G. Herzer, Soft magnetic nanocrystalline materials, Scr. Metall. Mater. 33 (1995) 1741–1756.
[22] G. Herzer, Modern soft magnets: amorphous and nanocrystalline materials, Acta Mater. 61 (2013) 718–734.
[23] A. Makino, H. Men, T. Kubota, K. Yubuta, A. Inoue, New Fe-metalloids based nanocrystalline alloys with high B_s of 1.9 T and excellent magnetic softness, J. Appl. Phys. 105 (2009) 013922.
[24] M. Ohta, Y. Yoshizawa, Magnetic properties of nanocrystalline Fe$_{82.65}$Cu$_{1.35}$Si$_x$B$_{16-x}$ alloys (x = 0–7), Appl. Phys. Lett. 91 (2007) 062513–062517.
[25] S. Takajo, Y. Kiyota, Analysis of high frequency magnetic properties of compressed iron powder cores, J. Jpn. Soc. Powder Powder Metall. 32 (7) (1985) 259–263.
[26] D.C. Jiles, Modeling the effects of eddy-current losses on frequency-dependent hysteresis in electrically conducting media, IEEE Trans. Magn. 30 (1994) 4326–4328.
[27] C. Serpico, C. Visone, I.D. Mayergoyz, V. Basso, G. Miano, Eddy current losses in ferromagnetic laminations, J. Appl. Phys. 87 (2000) 6923–6925.
[28] V. Leger, C. Ramiarinjaona, R. Barrue, R. Lebourgeois, Composite magnetic materials based on nanocrystalline powders for middle- and high-frequency applications up to 1 MHz, J. Magn. Magn. Mater. 191 (1999) 169–173.
[29] G. Ott, J. Wrba, R. Lucke, Recent developments of Mn-Zn ferrites for high permeability applications, J. Magn. Magn. Mater. 254 (2003) 535–537.
[30] V.T. Zaspalis, V. Tsakaloudi, M. Kolenbrander, The effect of dopants on the incremental permeability of MnZn-ferrites, J. Magn. Magn. Mater. 313 (2007) 29–36.